Metal–Organic Chemical Vapor Deposition of Copper and Copper(I) Oxide: Kinetics and Reaction Mechanisms in the Presence of Oxygen

Guglielmo G. Condorelli, Graziella Malandrino, and Ignazio Fragalà*

Dipartimento di Scienze Chimiche, Università di Catania, 95125 Catania, Italy

Received March 29, 1995. Revised Manuscript Received August 17, 1995[⊗]

The kinetics and the mechanisms of the deposition processes of copper and copper oxide by chemical vapor deposition from the Cu(acac)$_2$ precursor were studied in a horizontal-flow, low-pressure MOCVD reactor in the oxygen partial pressure range of 0–3.74 Torr. The nature and the deposition rate of films were determined under different operating conditions (e.g., reactant composition). At 573 K under high P_{O_2} and low $P_{Cu(acac)_2}$ values, copper(I) oxide is the main product. At low P_{O_2} and high $P_{Cu(acac)_2}$ values, metallic copper, containing carbon contamination, is formed. It is remarkable that for almost singular P_{O_2} and $P_{Cu(acac)_2}$ values (0.92 and 1.58 × 10^{-3} Torr, respectively) pure metallic copper free from carbon contaminations was obtained. A reaction mechanism based on the dissociative adsorption of Cu(acac)$_2$ on two different kinds of active sites has been proposed to explain the chemical nature of the films as well as the complex kinetics of the deposition process.

Introduction

Copper is a candidate to replace aluminum and tungsten for metallization in microelectronics, especially in very large-scale integrated (VLSI).[1,2] It offers advantages over both metals due to its lower electrical resistivity and to the greater structural integrity. Copper oxides have also been discussed as possible low-cost thin-film semiconductors in the fabrication of solar cells.[3–6]

Previous studies have demonstrated that good-quality copper films can be obtained by chemical vapor deposition (CVD) using various organometallic precursors. Processes based on the H$_2$ reduction of copper(II) β-diketonate complexes have been employed in the deposition of metallic copper,[7–15] while copper oxide based films have been obtained using Cu(II) complexes in the presence of oxygen.[16–20] More recently, metallic copper was obtained by processes based on the disproportionation of copper(I) complexes, based on β-diketonate compounds in which one ligand has been changed against a neutral ligand.[9,21–25]

In a previous paper[16] we have shown that below 593 K the rate of MOCVD growth of copper-containing films is governed by a surface reaction limited regime. Within this regime and in the oxygen partial pressure (P_{O_2}) range of 2.24–3.74 Torr, the copper deposition rate (r) increases with increasing Cu(acac)$_2$ precursor partial pressure ($P_{Cu(acac)_2}$) until a constant limit is obtained. Under these saturation conditions the deposition rate depends linearly on the oxygen partial pressure. In this higher pressure range the Cu deposition involves the dissociative adsorption of the Cu(acac)$_2$ precursor on surface-active sites. The adsorption process is irreversible, with the Cu atom becoming part of the film surface. The adsorbed ligands undergo decomposition into volatile byproducts when reacting with adsorbed O atoms. The kinetics of the entire deposition process obeys a relatively simple equation:

$$r = \frac{k'_1 k'_3 P_{O_2} P_{Cu(acac)_2}}{k'_1 P_{Cu(acac)_2} + k'_3 P_{O_2}} \qquad (I)$$

where k'_1 and k'_3 are, respectively, the rate constants of the Cu(acac)$_2$ adsorption and of the ligand decomposition processes.

The extension of experiments below the mentioned P_{O_2} range proved of particular relevance since a very

[⊗] Abstract published in *Advance ACS Abstracts,* October 1, 1995.

(1) Pai, P.; Ting, C. H. *IEEE Electron Device Lett.* **1989**, *10*, 423.
(2) Chamberlain, M. B. *Thin Solid Films* **1982**, *91*, 155.
(3) Rakhshani, A. E. *Solid State Electron.* **1986**, *29*, 7.
(4) Rai, B. P. *Sol. Cells* **1988**, *25*, 265.
(5) Olsen, L. C.; Addis, F. W.; Miller, W. *Sol. Cells* **1982–1983**, *7*, 247.
(6) Sears, W. M.; Fortin, E. *Sol. Energy Mater.* **1984**, *10*, 93.
(7) Dubois, L. H.; Zegarski, B. R. *J. Electrochem. Soc.* **1992**, *139*, 3295.
(8) Donnelly, V. M.; Gross, M. E. *J. Vac. Sci. Technol., A* **1993**, *11*, 66.
(9) Kaloyeros, A. E.; Fury, M. A. *MRS Bull.* **1993**, *18*, 22.
(10) Lecohier, B.; Calpini, B.; Philippoz, J. M.; van den Bergh, H.; Laub, D.; Buffat, P. A. *J. Electrochem. Soc.* **1993**, *140*, 789.
(11) Rees, W. S., Jr.; Caballero, C. R. *Adv. Mater. Opt. Electron.* **1992**, *1*, 59.
(12) Hoke, J. B.; Stern, E. W. *J. Mater. Chem.* **1991**, *1*, 701.
(13) Gerfin, T.; Becht, M.; Dahmen, K. H. *Mater. Sci. Eng., B* **1993**, *B17*, 97.
(14) Lai, W. G.; Xie, Y.; Griffin, G. L. *J. Electrochem. Soc.* **1991**, *138*, 3499.
(15) Griffin, G. L.; Maverick, A. W. In *The Chemistry of Metal CVD*; Kodas, T., Hampden-Smith, M., Eds.; VCH: Weinheim, Federal Republic of Germany, 1994; p 175.
(16) Condorelli, G. G.; Malandrino, G.; Fragalà, I. *Chem. Mater.* **1994**, *6*, 1861.
(17) Malandrino, G.; Richeson, D. S.; Marks, T. J.; DeGroot, D. C.; Schindler, J. L.; Kannewurf, C. R. *Appl. Phys. Lett.* **1991**, *58*, 182.
(18) Armitage, D. N.; Dunhill, N. I.; West, R. H.; Williams, J. O. *J. Cryst. Growth* **1991**, *108*, 683.
(19) Rees, W. S., Jr.; Caballero, C. R. *Mater. Res. Soc. Symp. Proc.* **1992**, *250*, 297.
(20) Chang, Y.; Schrader, G. L. *Mater. Res. Soc. Symp. Proc.* **1992**, *250*, 291.
(21) Jain, A.; Chi, K. M.; Kodas, T. T.; Hampden-Smith, M. J.; Farr, J. D.; Paffett, M. F. *Chem. Mater.* **1991**, *3*, 995.
(22) Shin, H. K.; Chi, K. M.; Hampden-Smith, M. J.; Kodas, T. T.; Farr, J. D.; Paffett, M. *Chem. Mater.* **1992**, *4*, 788.
(23) Cohen, S. L.; Liehr, M.; Kasi, S. *Appl. Phys. Lett.* **1992**, *60*, 50.
(24) Kumar, R.; Maverick, A. W. *Chem. Mater.* **1993**, *5*, 251.
(25) Shin, H. K.; Chi, K. M.; Hampden-Smith, M. J.; Kodas, T. T.; Farr, J. D.; Paffett, M. *Adv. Mater.* **1991**, *3*, 246.

0897-4756/95/2807-2096$09.00/0 © 1995 American Chemical Society

remarkable increase of the deposition rate has been observed, and this observation appears particularly attractive for technological applications. Moreover, the dependence of r upon P_{O_2} shows more intriguing patterns, thus suggesting more complex mechanisms.

In this perspective an extension of our early studies was needed and in this paper we report on thin–film deposition of Cu phases using the simple $Cu(acac)_2$ precursor.

Our attention has been focused on the deposition of Cu or Cu_2O by varying the reactant composition, namely, the O_2 and the $Cu(acac)_2$ partial pressure. The mechanism of the process has been studied using X-ray fluorescence and X-ray diffraction as well as X-ray and Auger photoelectron spectroscopies. This study is of relevance to design well-controlled synthetic procedures for metallic copper and copper oxides as well as for the development of other precursor based on β–diketonates.

Experimental Section

Deposition experiments were performed in a low-pressure, horizontal-flow, MOCVD reactor described elsewhere.[16] Films were deposited on glass slides placed on a boron nitride susceptor. The substrates were preliminarily cleaned with a saturated KOH solution, washed with bidistilled water and acetone and, finally, dried in air at 100 °C. Prepurified Ar (30 sccm) was used as carrier gas and a mixture Ar/O_2 (200 sccm) as reaction gas. Different oxygen partial pressures have been obtained by varying the O_2/Ar flow rate ratio keeping the total flow rate constant. The total pressure was held constant at 4.3 Torr using a MKS Baratron 122AAX system. The flow rates were controlled (within ±2 sccm) using MKS flow controllers and a MKS Multi gas Controller 147.

The bis(pentane-2,4-dionato)copper(II) precursor was purchased from Aldrich and was purified by low-pressure sublimation. IR and MS quality anhydrous material was warranted to preclude any possible cause of coformation of copper oxide films during depositions. In all the experiments weighed amounts of the precursor were moved from the cold presublimation section into the preheated sublimation section. The carrier gas was then flowed for different selected times. The total quantity of the sublimed precursor was determined by weight-loss measurements of the residual material.

The deposition rate ($\mu g\ cm^{-2}\ min^{-1}$) was determined by measuring the total quantity of copper deposited in a selected time. Quantitative analyses of Cu($\mu g/cm^2$) in the deposited material were made using a Philips PW 1410/00/60 wavelength-dispersive X-ray fluorescence spectrometer equipped with a tungsten anode and a LiF (220) crystal as secondary radiation-dispersive element. The intensities of Cu Kα peaks measured for several Cu and CuO_x MOCVD-deposited standards were used as calibration references. The absolute masses of the above-mentioned standards were determined by atomic absorption spectroscopy. The estimated error is on the order of 5%.

X-ray photoelectron spectra (XPS) and Auger depth profiles were obtained using a PHI 5600 Multy Technique System. The spectrometer was equipped with a monochromatic Al X-ray source operating at 400 W and with an electron gun operating at 8 kV. Sputter etching was made with a 2 kV argon ion gun with a beam current of 1 μA, having an incidence angle of 60° with the sample surface. The ion scan was rastered over a 3 × 3 mm area, in order to ensure the homogeneous erosion of thin layers. Accordingly depth profiles were obtained alternating Auger analysis focused within the crater and sputter etching steps.

X-ray diffraction (XRD) spectra were made using a Philips PW 1130 diffractometer equipped with a copper anode.

Suitable conditions for surface-reaction-rate limited processes were determined preliminarily as described elsewhere.[16] Figure 1 shows log plot of the dependence of the deposition rate (r) on the susceptor temperature at different oxygen partial pressures. According to our earlier paper,[16] the rate is surface-reaction limited below 593 K since the log r depends linearly on the reciprocal of the temperature. The deposition rate appears constant above 593 K, suggesting that the process is feed rate or diffusion rate limited. The deposition processes were, therefore, studied at 573 K susceptor temperature (surface-reaction-rate limited regime).

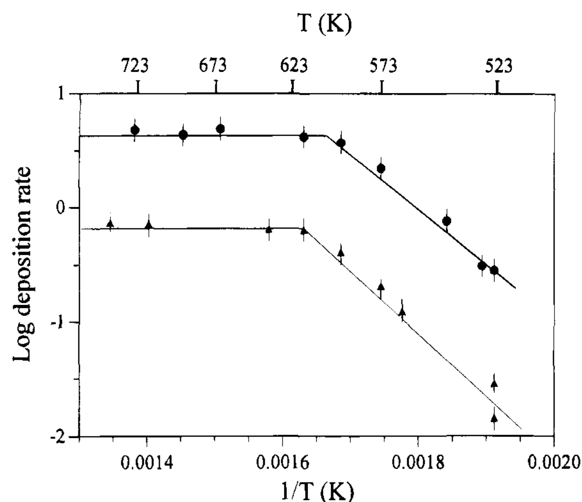

Figure 1. Arrhenius plots of deposition rate ($\mu g\ cm^{-2}\ min^{-1}$) vs $1/T$ ($1/K$) at P_{O_2} = 3.74 Torr (●) and P_{O_2} = 0 Torr (▲). Total pressure 4.3 Torr.

The LI.A.N.A. code[26] has been used throughout the fitting procedures. The code adopts PASCAL language compiled for MS DOS. The code solves linear and nonlinear fits, systems of equations, and function optimizations.

Results

Figures 2 and 3 show the dependence of the deposition rate (r) upon both P_{O_2} and $P_{Cu(acac)_2}$. Different trends are evident. In the 2.2 Torr $< P_{O_2} <$ 3.74 Torr range, r increases with the $P_{Cu(acac)_2}$ until a constant saturation limit for $P_{Cu(acac)_2}$ values higher than 1×10^{-3} Torr (Figure 3a). In this saturation range the reaction is zero order with respect to $Cu(acac)_2$ and the saturation limit value depends linearly on P_{O_2}, thus indicating that the reaction is also first order with respect to P_{O_2} (Figure 2). Complex trends are observed under lower P_{O_2} values. A marked trend toward greater growth rate values is observed upon decreasing P_{O_2} until a sharp maximum which, in turn, is followed by a sharp decrease. An analogous behavior is found as far as the dependence upon $P_{Cu(acac)_2}$ is concerned (Figure 3b,c).

To throw light on the deposition mechanisms, the nature of films deposited under various conditions has been investigated by X-ray photoelectron spectroscopy, Auger depth profiles, and XRD measurements. Figure 4 shows depth profiles of films deposited under 0.92 Torr P_{O_2} upon varying $P_{Cu(acac)_2}$. It becomes evident (Figure 4a) that films deposited at low $P_{Cu(acac)_2}$ (0.87×10^{-3} Torr, films A in Figure 3c) are made of copper and oxygen without carbon contaminations in the bulk. The depth profiles of films (C in Figure 3c) obtained under higher $P_{Cu(acac)_2}$ (1.91×10^{-3} Torr) show traces of carbon contaminations in the bulk. Moreover the lack of any defined plateau in the middle of the depth profile suggests that the deposition process does not occur

(26) We thank P. Mineo, C. Rigano, and S. Sammartano (Dipartimento di Chimica Inorganica, Analitica e Struttura Molecolare Università di Messina, Salita Sperone, Sant'Agata di Messina, Messina) for providing the LI.A.N.A. code.

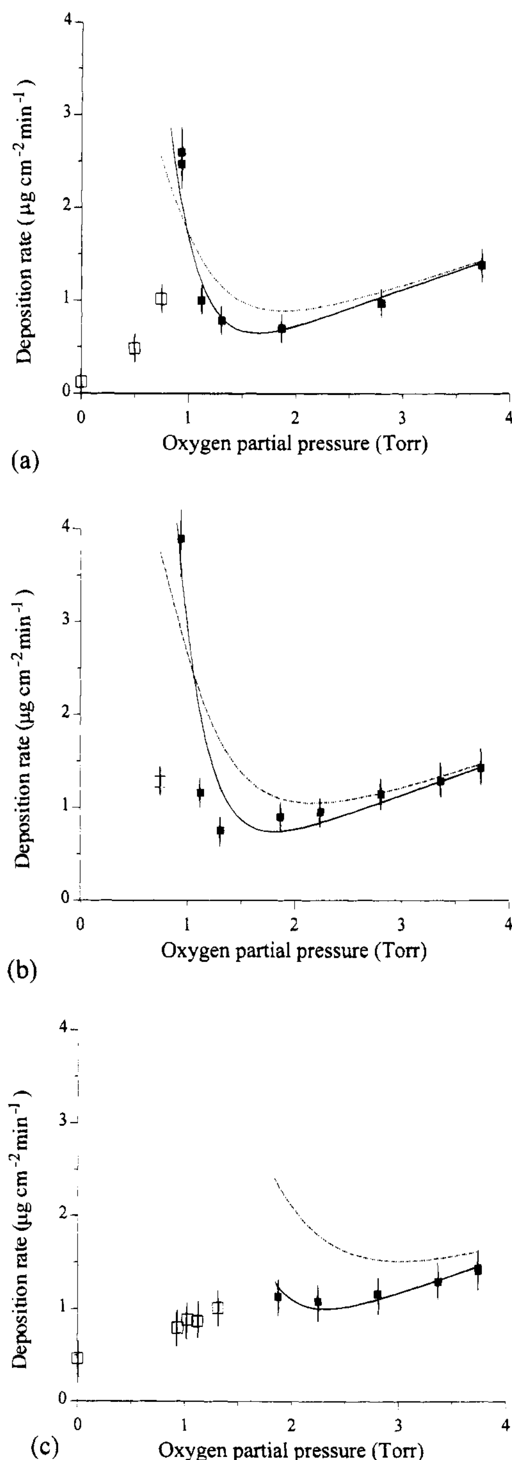

Figure 2. Dependence of deposition rate ($\mu g\ cm^{-2}\ min^{-1}$) on oxygen partial pressure at various Cu(acac)$_2$ partial pressures. (a) $P_{Cu(acac)_2} = 0.87 \times 10^{-3}$ Torr; (b) $P_{Cu(acac)_2} = 1.6 \times 10^{-3}$ Torr; (c) $P_{Cu(acac)_2} = 7.75 \times 10^{-3}$ Torr. (■) Carbon-free films; (□) carbon-contaminated films. The solid curves represent theoretical data obtained from the two-step model. Dashed curves relate to the one-step model. Theoretical curves are plotted only in the carbon-free region.

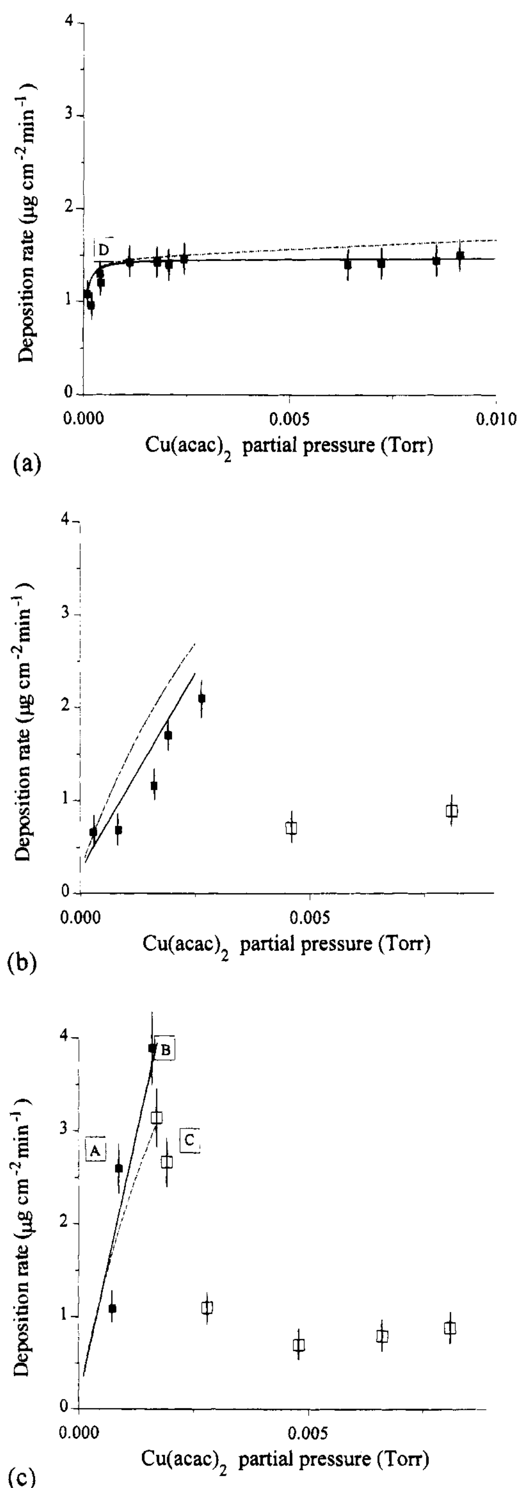

Figure 3. Dependence of the deposition rate ($\mu g\ cm^{-2}\ min^{-1}$) on Cu(acac)$_2$ partial pressure at various oxygen partial pressures. (a) $P_{O_2} = 3.74$ Torr; (b) $P_{O_2} = 1.12$ Torr; (c) $P_{O_2} = 0.92$ Torr. (■) Carbon-free films; (□) carbon-contamined films. The solid curves represent theoretical data obtained from the two-step model. Dashed curves relate to the one-step model. Theoretical curves are plotted only in the carbon-free region. The [A], [B], [C], and [D] notations refer to films investigated by AES, XPS, and XRD (Figures 4–6).

under steady state conditions (Figure 4c). At $P_{Cu(acac)_2} = 1.58 \times 10^{-3}$ Torr films (B in Figure 3c) are made of copper with no carbon or oxygen contamination in the bulk (Figure 4b). Note that in these conditions the copper deposition rate reaches a maximum value (Figure 3c). Under higher P_{O_2} values (3.74 Torr, film D in Figure 3a) a parallel evolution of the Cu and O atomic composition is observed (Figure 4d) with no carbon contamination. This is a clear indication of a massive copper oxidation. The absence of oxygen in the reacting gas (P_{Ar} = 4.3 Torr), finally, results in films having notable carbon contaminations (Figure 4e).

The chemical nature of copper phases was investigated by XPS since it is well known that the energies

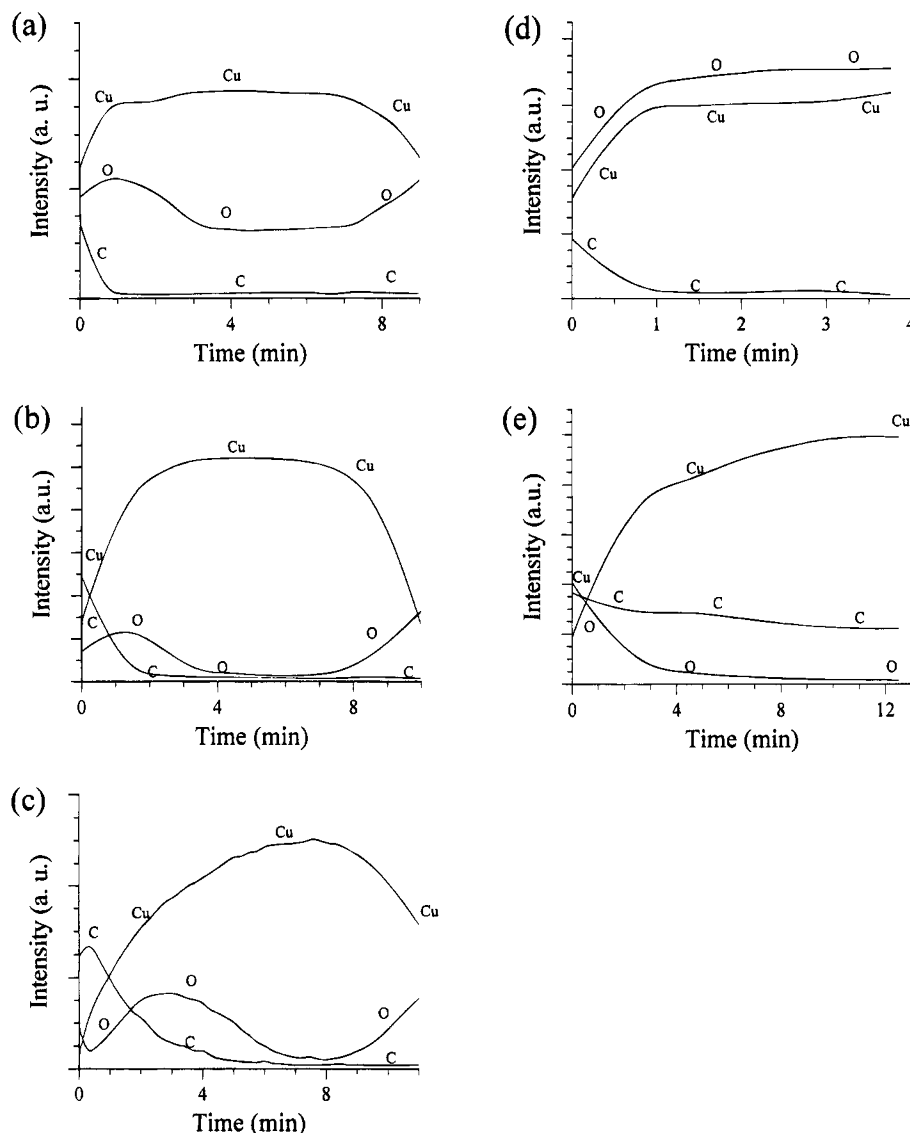

Figure 4. Auger depth profiles of films deposited under various conditions. (a) $P_{Cu(acac)_2} = 0.87 \times 10^{-3}$ Torr, $P_{O_2} = 0.92$ Torr; (b) $P_{Cu(acac)_2} = 1.58 \times 10^{-3}$ Torr, $P_{O_2} = 0.92$ Torr; (c) $P_{Cu(acac)_2} = 1.91 \times 10^{-3}$ Torr, $P_{O_2} = 0.92$ Torr; (d) $P_{Cu(acac)_2} = 0.55 \times 10^{-3}$ Torr, $P_{O_2} = 3.74$ Torr; (e) $P_{Cu(acac)_2} = 1.7 \times 10^{-3}$ Torr, $P_{O_2} = 0$ Torr. The deposition rates of films (a), (b), (c), and (d) are indicated in Figure 3 by points [A], [B], [C], and [D], respectively.

associated with Cu 2p core ionization and Cu LMM Auger peaks are diagnostic of the oxidation state of Cu−O phases. Thus, Cu $2p_{3/2}$ peaks associated with Cu^{I} and Cu^{0} species have almost the same binding energies (BE) (932.5 and 932.7 eV, respectively) while the binding energy of Cu^{II} $2p_{3/2}$ peak is 933.6 eV.[27] Auger LMM peaks range from 570.1 eV (kinetic energy = 916.5 eV) for Cu^{I} to 568.8 eV (kinetic energy = 917.8 eV) for Cu^{II} and 568 eV (kinetic energy = 918.6 eV) Cu^{0}.[27] Moreover, the shakeup peak (940−944 eV) associated with the Cu $2p_{3/2}$ peak is a clear indication of the presence of CuO.[27] However, this indicator might not be highly diagnostic of the presence of a vertically uniform CuO phase in the films since the same phase has been found ubiquitous as a near-surface contamination of Cu phases. In this context, surface XPS spectra of as-deposited films grown under various Ar/O_2 ratios show massive shakeup peaks in the 940−944 eV BE range. Ar ion sputtering and subsequent XPS analysis provide an indication of the distribution of the metal and of the oxide phases since it is known that Ar-ion bombardment induces a $Cu^{II} \rightarrow Cu^{I}$ reduction[28] but not the $Cu^{I} \rightarrow Cu^{0}$ process. Thus, the shapes and energy positions (Figure 5d) of Cu $2p_{3/2}$ and Cu LMM peaks (BE = 932.5 eV and KE = 916.5 eV, respectively), observed after 6 min sputtering on film D in Figure 3a deposited at high P_{O_2} (3.74 Torr), are indicative of the presence of copper oxide. Moreover the XRD analysis of the same film (Figure 6d) has provided evidence of Cu_2O alone. Even at high $O_2/Cu(acac)_2$ mole ratio no traces of CuO have been detected. Films made under lower partial pressures (0.92 Torr, films A in Figure 3c) consist of both metallic copper and copper(I) oxide (Figure 5a), while films deposited under the same P_{O_2} and higher $P_{Cu(acac)_2}$ (C in Figure 3c) are made of metallic copper with carbon contamination (Figures 4c and 5c). Finally, films deposited under pure Ar-reacting gas have only metallic copper content with notable carbon contamination (Figures 5e and 4e). It is worthy of note that films B in Figure 3c only show XPS and Auger features (Cu $2p_{3/2}$ at BE = 932.6 eV and Cu LMM at KE = 918.6 eV)

(27) Deroubaix, G.; Marcus, P. *Surf. Interface Anal.* **1992**, *18*, 39.

(28) Mitchell, D. F.; Sproule, G. I.; Graham, M. J. *Surf. Interface Anal.* **1990**, *15*, 487.

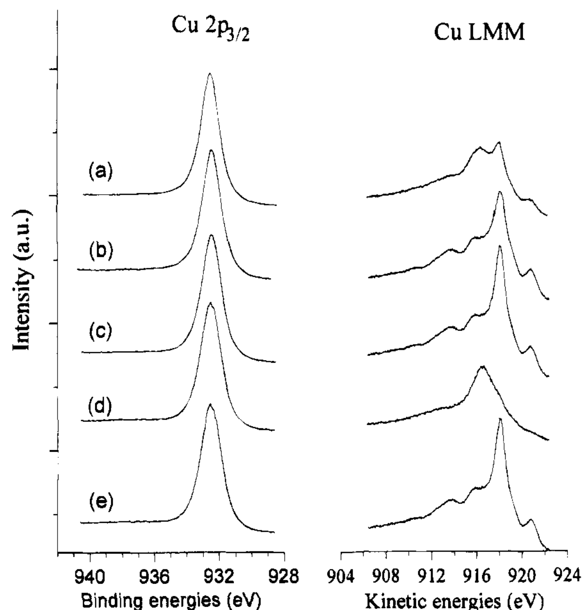

Figure 5. XPS Cu $2p_{3/2}$ and the Cu LMM peaks after 6 min sputtering of films deposited under various conditions. (a) $P_{Cu(acac)_2} = 0.87 \times 10^{-3}$ Torr, $P_{O_2} = 0.92$ Torr; (b) $P_{Cu(acac)_2} = 1.58 \times 10^{-3}$ Torr, $P_{O_2} = 0.92$ Torr; (c) $P_{Cu(acac)_2} = 1.91 \times 10^{-3}$ Torr, $P_{O_2} = 0.92$ Torr; (d) $P_{Cu(acac)_2} = 0.55 \times 10^{-3}$ Torr, $P_{O_2} = 3.74$ Torr; (e) $P_{Cu(acac)_2} = 1.7 \times 10^{-3}$ Torr, $P_{O_2} = 0$ Torr. The deposition rates of films (a), (b), (c), and (d) are indicated in Figure 3 by points [A], [B], [C], and [D], respectively.

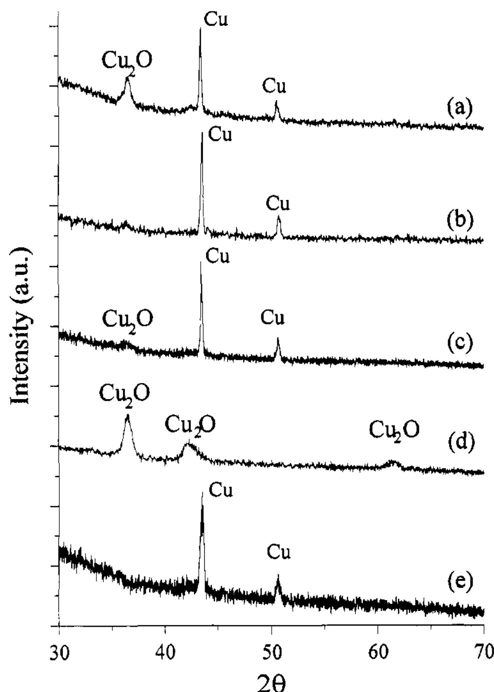

Figure 6. XRD spectra of films deposited under various conditions. (a) $P_{Cu(acac)_2} = 0.87 \times 10^{-3}$ Torr, $P_{O_2} = 0.92$ Torr; (b) $P_{Cu(acac)_2} = 1.58 \times 10^{-3}$ Torr, $P_{O_2} = 0.92$ Torr; (c) $P_{Cu(acac)_2} = 1.91 \times 10^{-3}$ Torr, $P_{O_2} = 0.92$ Torr; (d) $P_{Cu(acac)_2} = 0.55 \times 10^{-3}$ Torr, $P_{O_2} = 3.74$ Torr; (e) $P_{Cu(acac)_2} = 1.7 \times 10^{-3}$ Torr, $P_{O_2} = 0$ Torr. The deposition rates of films (a), (b), (c), and (d) are indicated in Figure 3 by points [A], [B], [C], and [D], respectively.

typical of metallic copper with no carbon contamination (Figures 5b and 4b). Similar indication can be arrived at by XRD analysis of the same films (Figure 6). Hence, the present report represents the first evidence of pure metallic copper through a real MOCVD process using $Cu(acac)_2$ and O_2 as reagents. In this context, it must be noted that Hammadi et al.[29] have reported on the deposition of Cu(0) films via a process resembling MOCVD conditions under different $P_{Cu(acac)_2}/P_{O_2}$ ratio. The films were, however, carbon contaminated since in situ Auger spectra were showing evidence of the KLL carbon peak.

Finally, we note that deposition of films with no carbon contamination occurs (Table 1) in steady-state conditions (constant deposition rate). By contrast, carbon contamination results in the poisoning of the surface since slower deposition rates are observed upon increasing the deposition time (Table 1).

Discussion

Present results have shown that very low P_{O_2} as well as high $P_{Cu(acac)_2}$ cause carbon contamination in the films, thus preventing steady-state deposition regimes (Table 1). In particular the observed slower deposition rates, as well as the decreasing trend observed upon increasing the deposition time (vide infra), suggest that carbon contaminations result in the poisoning of active sites on the surface. Carbon, therefore, is likely formed because of the incomplete combustion of the adsorbed reagents when P_{O_2} is not enough for decomposition in volatile byproducts. The effect of the carbon contamination on the deposition rate can explain the complex shape of the Auger depth profile in Figure 4c. Under those conditions there is evidence of metallic copper in the deeper layers. Remarkable carbon contaminations are, by contrast, formed upon increasing the deposition time. This greater contamination results in a decreased deposition rate (Table 1) and, in turn, in a greater Cu_2O formation due to a layer-by-layer oxidation faster than the growth of the Cu phase.[16]

The conditions suitable to avoid carbon contaminations become of major interest both because of possible practical applications of carbon-free films as well as of possible applications of the steady-state approximation (hence of mathematical models) to explain experimental results. In this context a schematic rationale to the mechanisms related to the deposition of carbon-free films can be proposed within the frame of the earlier reaction pathway proposed for CuO_x.

In this context two different sites (on the copper(I) oxide (A) and on the copper metal (C) surfaces) are expected for $Cu(acac)_2$ adsorption which, in turn, can occur either in one or two steps:

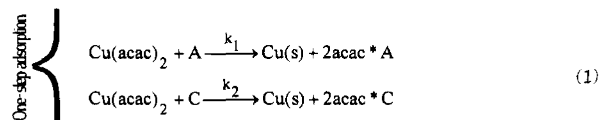

(1)

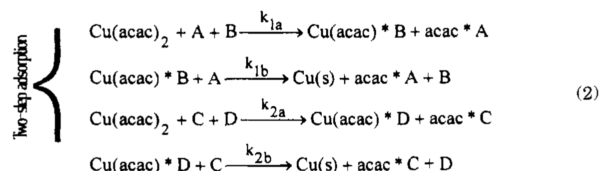

(2)

(29) Hammadi, Z.; Lecohier, B.; Dallaporta, H. *J. Appl. Phys.* **1993**, *73*, 5213.

Table 1. Dependence of the Deposition Rate on the Deposition Time

films with no carbon contaminations, $P_{O_2} = 3.74$ Torr; $P_{Cu(acac)_2} = 1.8 \times 10^{-3}$ Torr		films with carbon contaminations, $P_{O_2} = 0.75$ Torr; $P_{Cu(acac)_2} = 1.5 \times 10^{-3}$ Torr	
deposition time (min)	rate (μg cm^{-2} min^{-1})	deposition time (min)	rate (μg cm^{-2} min^{-1})
10	1.42	25	1.41
30	1.44	51	1.27
62	1.43	75	0.77

Note that in the two-step adsorption mechanism it becomes necessary to add two more kinds of active sites (types B and D) to account for adsorption of Cu(acac)* species because the Cu(acac) and acac surface species may adsorb with different mechanisms.[30,31]

In accordance with earlier data, oxygen reversibly adsorbs on active sites of type E and, then, reacts with adsorbed ligands to produce volatile byproduct:

$$O_2 + 2E \overset{K_e}{\longleftrightarrow} 2O*E \qquad (3)$$

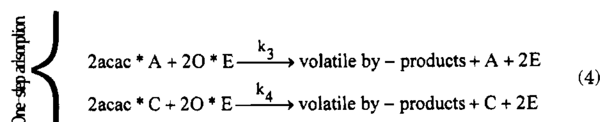

$$2acac*A + 2O*E \xrightarrow{k_3} \text{volatile by-products} + A + 2E$$
$$2acac*C + 2O*E \xrightarrow{k_4} \text{volatile by-products} + C + 2E \qquad (4)$$

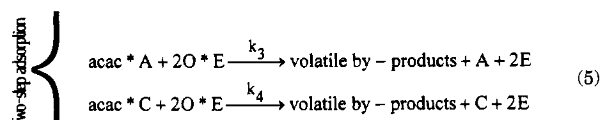

$$acac*A + 2O*E \xrightarrow{k_3} \text{volatile by-products} + A + 2E$$
$$acac*C + 2O*E \xrightarrow{k_4} \text{volatile by-products} + C + 2E \qquad (5)$$

Moreover the copper metal surface (S_{Cu}) undergoes oxidation by adsorbed O atoms with the net result that part of the active sites C and D are transformed in the sites A and B on the copper(I) oxide surface:

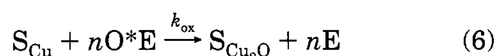

$$S_{Cu} + nO*E \xrightarrow{k_{ox}} S_{Cu_2O} + nE \qquad (6)$$

where n represents the number of oxygen atoms involved in the process itself and S_{Cu_2O} is the copper oxide surface.

Finally O_2 can adsorb selectively on sites C on the metallic surface, thus competing with $Cu(acac)_2$:

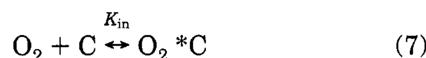

$$O_2 + C \overset{K_{in}}{\leftrightarrow} O_2*C \qquad (7)$$

An analogous competition does nor occur on sites A on the Cu_2O surface in accordance with earlier results.[16]

Two different kinetic expressions can be obtained depending upon the reaction scheme (one-step or two-step) adopted (see Appendix). In addition, the fraction of Cu^0 in the films can also be obtained from the same model (see Appendix). The experimental dependence of the Cu^0 fraction upon the oxygen partial pressure is shown in Figure 7 and compared with calculated values. A close accordance of the experimental results with model calculations is evident. Therefore in the absence of O_2, contaminated Cu metal films are formed. At low P_{O_2}, there is sufficient O_2 to oxidize the ligands to give copper films. At higher P_{O_2}, the reaction of O_2 with deposited copper becomes more significant thus resulting in the formation of copper(I) oxide. In this context it is noted that a quantitative estimation of the Cu^0 fraction in the films containing only Cu^0 and/or Cu^I phases can be obtained using the approach reported in earlier studies.[32,33] Therefore the Cu^0 atomic fraction has been derived from the Cu LMM peak heights (at KE = 918.6 and 916.5 eV) measured above a linear background from 890 to 924 eV.

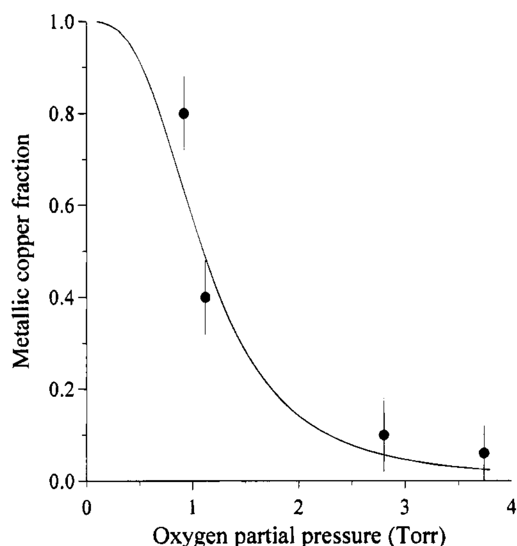

Figure 7. Dependence of the fraction of metallic copper upon the oxygen partial pressure at $P_{Cu(acac)_2} = 1.5 \times 10^{-3}$ Torr. (●) Experimental points. The solid line represents theoretical data.

To provide a better test for the validity of the proposed models, a simultaneous fit of experimental values of both the deposition rate and the metallic copper fraction has been made. The comparisons between experimental data and the kinetic equations obtained from the proposed reaction scheme are shown in Figures 2, 3, and 8. Quantitative percentual mean deviations and values of kinetic parameters are reported as supporting information (Tables S1–3) depending upon the model adopted. The two-step process provides the best fit with the experimental data, while the one-step process provides a less adequate quantitative description of the deposition processes. It should be noted, in addition, that better fits are obtained for greater numbers of adsorbed oxygen atoms involved in the oxidation process (see text step (6)).

Finally, we comment on the deposition rate equations obtained from the present modellistic approach (eqs IX and XIII in Appendix). There is no doubt that they represent a more comprehensive extension of our earlier model[16] proposed for depositions under high P_{O_2}. It turns out, in fact, that for high P_{O_2} values, r_{tot} can be

(30) Kodas, T.; Hampden-Smith, M. In *The Chemistry of Metal CVD*; Kodas, T., Hampden-Smith, M., Eds.; VCH: Weinheim, Federal Republic of Germany, 1994; p 239.
(31) Girolami, G. S.; Jeffries, P. M.; Dubois, L. H. *J. Am. Chem. Soc.* **1993**, *115*, 1015.
(32) Moretti, G.; Fierro, G.; Lo Jacono, M.; Porta, P. *Surf. Interface Anal.* **1989**, *14*, 325.
(33) Apai, G.; Monnier, J. R.; Hanrahan, M. J. *Appl. Surf. Sci.* **1984**, *19*, 307.

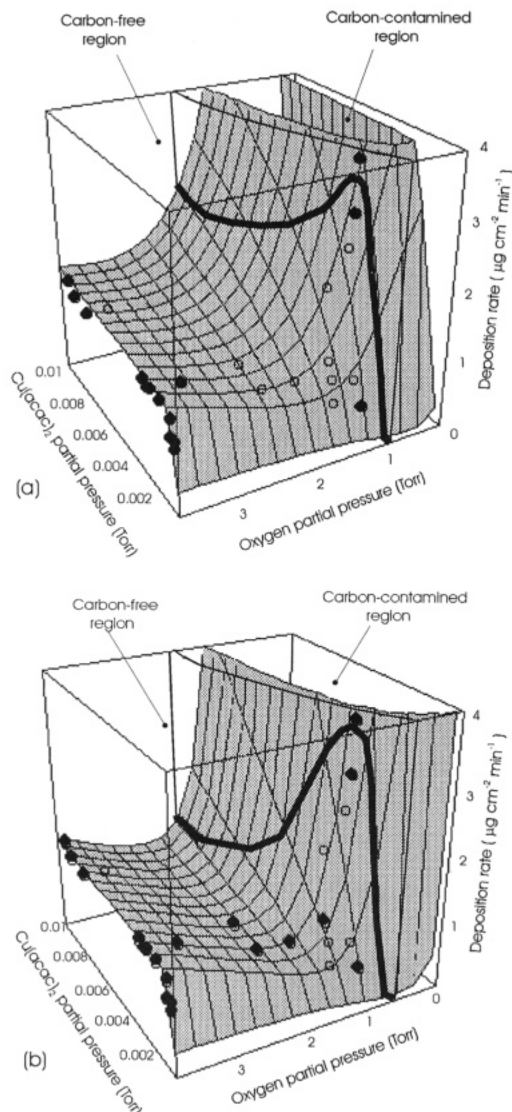

Figure 8. Best-fit surfaces of (a) one-step model, (b) two-step model. (●, ○) Experimental points above and behind the fit surfaces, respectively. The bold solid curves on the surfaces indicate the boundary between the carbon-free and the carbon-contamined regions.

simplified as:

$$r_{\rm tot} = r_{\rm 1b} = r_1 = \frac{k'_1 k'_3 P_{\rm O_2} P_{\rm Cu(acac)_2}}{a k'_1 P_{\rm Cu(acac)_2} + k'_3 P_{\rm O_2}} \qquad \text{(II)}$$

with $a = 1$ or 2 for the one-step or the two-step model, respectively.

Conclusions

In the present paper the kinetics and the phenomenology of Cu-phase deposition under MOCVD conditions have been investigated. Experimental parameters that govern the formation either of the Cu_2O phase or of pure Cu metal have been settled. Moreover, conditions to avoid carbon contamination have been determined as well.

A schematic reaction mechanism has been proposed to account for the complex phenomenology of the deposition process. The mechanism is based upon the dissociative adsorption of precursors on the surface. The ligands adsorbed on the film surface are then decomposed into volatile byproducts by adsorbed oxygen atoms and, at higher oxygen partial pressure, the oxidation rate of metallic copper becomes high enough to allow massive formation of copper(I) phase.

Kinetic analyses have been developed for both the one-step and the two-step processes. The expressions obtained for the two-step process provide the best fit with the experimental data of both deposition rate and metallic copper fraction in the films.

Acknowledgment. Professor G. Marletta (Department of Chemistry, University of Catania) is gratefully acknowledged for helpful discussion. We gratefully thank the Ministero dell'Università e della Ricerca Scientifica e Tecnologica (MURST Rome, Italy) for financial support.

Appendix

Symbols adopted along with the model presently used:

$S_{i(i={\rm A,C})}$ = surface density of active sites i in the copper oxide

$S_{i(i={\rm B,D})}$ = surface density of active sites i in the copper metal

$\theta_{i(i={\rm A,B,C,D})}$ = fraction of active sites i unoccupied

$\theta_{\rm Cu}$ = fraction of surface covered by copper metal

$1 - \theta_{\rm Cu}$ = fraction of surface covered by copper oxide

K_i = equilibrium constant

k_i = kinetic constant

In the *one-step process*, the deposition rate on copper oxide (r_1) and on metal copper (r_2) are

$$r_1 = k_1 S_{\rm A} \theta_{\rm A} P_{\rm Cu} = k'_1 \theta_{\rm A} P_{\rm Cu} \qquad \text{(III)}$$

$$r_2 = k_2 S_{\rm C} \theta_{\rm C} P_{\rm Cu} = k'_2 \theta_{\rm C} P_{\rm Cu} \qquad \text{(IV)}$$

From steps (3), (4), and (7) and assuming negligible the fraction of active sites E occupied by adsorbed oxygen atoms, the rates of ligands decomposition are

$$r_3 = k_3 K_{\rm e} P_{\rm O_2} S_{\rm A}(1 - \theta_{\rm Cu} - \theta_{\rm A}) = k'_3 P_{\rm O_2}(1 - \theta_{\rm Cu} - \theta_{\rm A}) \qquad \text{(V)}$$

$$r_4 = k_4 K_{\rm e} P_{\rm O_2} S_{\rm C}(\theta_{\rm Cu} - \theta_{\rm C} - K_{\rm in} P_{\rm O_2} \theta_{\rm C}) = k'_4 P_{\rm O_2} (\theta_{\rm Cu} - \theta_{\rm C} - K_{\rm in} P_{\rm O_2} \theta_{\rm c}) \qquad \text{(VI)}$$

on Cu_2O (r_3) and Cu (r_4) surfaces respectively.

From steps (3) and (6) the oxidation rate is

$$r_{\rm ox} = k_{\rm ox} K_{\rm e}^{n/2} \theta_{\rm Cu} P_{\rm O_2}^{\ n/2} = k'_{\rm ox} \theta_{\rm Cu} P_{\rm O_2}^{\ n/2} \qquad \text{(VII)}$$

In steady-state conditions

$$\begin{cases} {\rm d}\theta_{\rm A}/{\rm d}t = 0 \\ {\rm d}\theta_{\rm C}/{\rm d}t = 0 \\ {\rm d}\theta_{\rm Cu}/{\rm d}t = 0 \end{cases} \Rightarrow \begin{cases} r_1 = r_3 \\ r_2 = r_4 \\ r_1 = r_{\rm ox} \end{cases} \qquad \text{(VIII)}$$

From eqs III−VIII the decomposition rate is

$$r_{tot} = r_1 + r_2 \qquad \text{(IX)}$$

where

$$r_1 = k'_1 k'_3 k'_{ox} P_{Cu} P_{O_2}{}^{(n/2)+1} / \Lambda_1$$

$$r_2 = k'_1 k'_2 k'_3 k_4' P_{Cu}{}^2 P_{O_2}{}^2 / \Theta \Lambda_1$$

$$\Theta = k'_2 P_{Cu} + k'_4 P_{O_2} + k'_4 K'_{in} P_{O_2}{}^2$$

$$\Lambda_1 = k'_1 k'_3 P_{Cu} P_{O_2} + k'_1 k'_{ox} P_{Cu} P_{O_2}{}^{n/2} + k'_3 k'_{ox} P_{O_2}{}^{(n/2)+1}$$

In the *two-step process* different expressions must be assumed for r_1 and r_2:

$$r_1 \Rightarrow \begin{cases} r_{1a} = k_{1a} S_A \theta_A S_B \theta_B P_{Cu} \approx k'_1 \theta_A (1 - \theta_{Cu}) P_{Cu} \\ r_{1b} = k_{1b} S_A \theta_A [\mathrm{Cu(acac)^*B}] \end{cases} \qquad \text{(X)}$$

$$r_2 \Rightarrow \begin{cases} r_{2a} = k_{2a} S_C \theta_C S_D \theta_D P_{Cu} \approx k'_2 \theta_C \theta_{Cu} P_{Cu} \\ r_{2b} = k_{2b} S_C \theta_C [\mathrm{Cu(acac)^*D}] \end{cases} \qquad \text{(XI)}$$

where the fractions of active sites B and D occupied by Cu(acac)* species have been assumed negligible with respect to the copper oxide and copper metal surfaces.

In addition two more steady-state conditions must be operating:

$$\begin{cases} \mathrm{d[Cu(acac)^*B]}/\mathrm{d}t = 0 \\ \mathrm{d[Cu(acac)^*D]}/\mathrm{d}t = 0 \end{cases} \Rightarrow \begin{cases} r_{1a} = r_{1b} \\ r_{2a} = r_{2b} \end{cases} \qquad \text{(XII)}$$

From eqs V−VIII and X−XII and neglecting the second-order term in θ_{Cu}, the deposition rate is

$$r_{tot} = r_{1b} + r_{2b} \qquad \text{(XIII)}$$

where

$$r_{1b} = k'_1 k'_3 k'_{ox} P_{Cu} P_{O_2}{}^{(n/2)+1} / \Lambda_2$$

$$r_{2b} = k_1'^2 k'_2 k_3'^2 k'_4 P_{Cu}{}^3 P_{O_2}{}^2 / \Gamma \Lambda_2$$

$$\Lambda_2 = k'_1 k'_3 P_{Cu} P_{O_2} + 2 k'_1 k'_{ox} P_{Cu} P_{O_2}{}^{n/2} + k'_3 k'_{ox} P_{O_2}{}^{(n/2)+1}$$

$$\Gamma = 2 k'_1 k'_2 k'_3 P_{Cu}{}^2 + k'_4 \Lambda_2 + k'_4 K'_{in} P_{O_2} \Lambda_2$$

The fraction θ_{Cu} of metallic copper for both one-step and two-step processes can also be obtained from eqs III−VIII, X, and XII:

$$\theta_{Cu} = k'_1 k'_3 P_{Cu} P_{O_2} / \Lambda_i \qquad \text{(XIV)}$$

where i = 1, 2 for one-step and two-step processes, respectively.

Supporting Information Available: Tables of best-fit indexes and parameters (1 page). Ordering information is given on any current masthead page.

CM9501473